Available online at www.elixirpublishers.com (Elixir International Journal)

Geoscience

Elixir Geoscience 64 (2013) 19447-19453

ISSN: 2229-712X

FMI farcies and reservoir characteristics of Kangan Formation, in South Pars gas field, south of Iran

Vafaei Hoshang[1,*], Rahimpoor-Bonab Hossain[2] and Jahani Davood[1]

[1]Department of Geology, College of Science, Islamic Azad University of north Tehran branch, Tehran, Iran.

[2]Department of Geology, College of Science, University of Tehran, Tehran, Iran.

ARTICLE INFO

Article history:

Received: 27 October 2013;
Received in revised form:
15 November 2013;
Accepted: 26 November 2013;

Keywords

Kangan formation,
FMI, Image log,
Facies pattern,
Reservoir characteristics,
Sequence stratigraphy.

ABSTRACT

The FMI (Fullbore formation microimager) log provides clear identification of wells geological characteristics. In this study, the identification and interpretation of the structures, texture, lithology, porosity, bedding, lamination, diagenetic processes, porous/non porous layers and determination of facies, sequence stratigraphy and reservoir characteristics in kangan formation, are discussed using FMI logs, thin section, core photograph and porosity logs. The Kangan lower Triassic aged carbonates formation, was deposited in the giant South Pars gas field in the Persian Gulf Basin and consists of limestone, dolomite, anhydritic dolomite, and thin shaly layers facies. The aim of this study is to provide the FMI farcies, sequence stratigraphy and subunits reservoir characteristics changes of Kangan Formation. Based on FMI logs and comparing with thin section, core photograph and porosity logs introduced 12 FMI facies(FF) in kangan formation (Table1). Three major composite depositional sequences have then been defined: K_1A, K_1B and K_2A. They have been further subdivided into 12 depositional units, 6 tight (low reservoir characteristics) and 6 conductive (high reservoir characteristics).

Introduction

The South Pars gas field along with its southern extension in Qatar (North field) forms the largest known natural gas accumulation which is located in the Persian Gulf (Fig.1). The Iran's share of this natural gas reserve is about 464 trillion cubic feet which is 8 percent of the entire world natural gas and 40 percent of Iran's total gas reserve (Aali et.al, 2001). The Kangan early Triassic aged carbonates (equivalents of the upper Khuff Formation) consists of limestone, dolomite, anhydritic dolomite, and thin shaly layers and is subdivided into two distinct reservoir units including the K_1 and K_2 (Szabo, and Kheradpir, 1978). Many authors have been studied Kangan formation (Rahimpour-Bonab, 2007; Moradpour M, et.al, 2008; Rahimpour-Bonab et al., 2009; Rahimpour-Bonab and Esrafili-Dizaji, 2009; Tavakoli, Rahimpour-Bonab and Esrafili-Dizaji, 2011; Esrafili-Dizaji and Rahimpour-Bonab 2013).

The Fullbore Formation Microimager (FMI) is a resistivity measuring tools that provide various images of sedimentary bodies and bed boundaries, rock textures, structures and pore system. It could present porosity distribution and permeability evolution (Schlumberger, 1992). FMI provide information on clays, bioclasts, calcite crystals, pores, fractures, stylolites, bedding, bioturbate textures, and other geological features in reservoirs and can be used for discriminating sedimentary facies, sequence boundaries, reservoir characteristics recognition and lithologies (Serra, 1989; Lovell et al., 1997; Prensky, 1999; Russell et al., 2002). Structural features such as faults and folds can also be clearly identified (Prilliman et al., 1997). In addition, they are sensitive to dissolution pores and cracks and can be used to estimate porosity, permeability, and other parameters (Nurmi et al., 1990; Standen et al., 1993; Newberry et al., 1996).

Our main goal in this study is to understand and discriminate facies, sequence stratigraphy and reservoir characteristics changes of the Knagan Formation by integration of FMI logs with thin section, core photograph and porosity logs.

Tools and Database

The FMI tools consists of 4 arms, 4 flaps and 4 pads (each arm supported by one pad and one flap), 192 electrodes with coverage up to 80 percent in 8.5 inch diameter borehole and provide a clear image of the rocks on all sides of the wellbore by measuring resistivity. Variations on these resistivity images reflect changing physical and chemical properties of the rock, such as porosity, mineralogy, cementation, and grain size. Typically FMI images are combined with conventional data for geological feature recognition (Schlumberger, 1992). During logging, each microelectrode emits a focused current into the formation. The button current intensity measurements, which reflect micro resistivity variations, are converted to variable intensity color images with identical horizontal and vertical scale (Schlumberger, 1991; Hammes, 1997). The images produce borehole wall picture, which allows detection of fine scale geological features with excellent vertical resolution (Bhavana et.al, 2004).

This study dataset consists of FMI logs, core photograph and thin sections in three wells from of Kangan Formation. Available data for wells 1 and 2 are thin sections, core photographs, FMI log and porosity diagrams, but for well 3 is FMI log and porosity diagrams.

Geological setting and stratigraphy

The South Pars field is a part of the huge NNE–SSW trending Qatar Arch structural feature. This region is located in

Tele:
E-mail addresses: h_vafaei1352@yahoo.com

the interior platform of the Arabian Plate and bounded by the Zagros folded belt to the north and northeast (Ziegler 2001; Konyuhov and Maleki 2006). Geology and reservoir characterization of South Pars Gas field and its southern extension, the North Dome, are well-documented by Alsharhan, 1993; Al-Jallal, 1994; Alsharhan and Naim, 1997; Rahimpour-Bonab, 2007; Moradpour M, et.al, 2008; Esrafili-Dizaji and Rahimpour-Bonab, 2009; Rahimpour-Bonab et al., 2009; Rahimpour-Bonab et al., 2010; Tavakoli, Rahimpour-Bonab and Esrafili-Dizaji, 2011; Esrafili-Dizaji and Rahimpour-Bonab, 2013. In the South Pars field, the Kangan Triassic stratigraphic unit is one of gas accumulation limited (Kashfi, 1992) and composed of a carbonate–evaporite series that is known regionally as the Khuff Formation (Alsharhan and Naim, 1997; Kashfi, 2000). This formation limited with Dalan (bottom) and Dashtak(top) that is an efficient cap rock and consists of two members including K_2 (limestone and dolomite) and K_1 (anhydritic dolomite, dolomite and limestone) (Fig2). The Persian Gulf Basin comprises several NW–SE-trending geotectonic units, such as the Arabian platform, and a zone of marginal troughs, including the Zagros fold belt, limited to the NE by the main Zagros reverse fault (Edgell 1996). Several important north–south structures, such as the major Qatar–Kazerun lineament (Qatar Arch), cross the region.

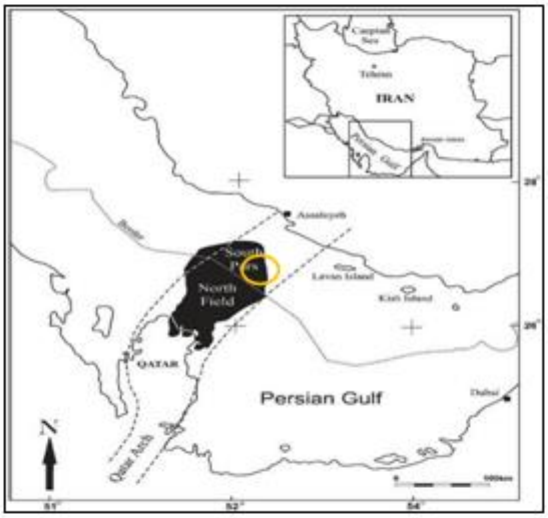

Fig 1: Location map of study wells and South Pars gas field, the Persian Gulf

Discussion and results

The FMI resistivity-difference based images from studied wells have been analysed to extract a description of sedimentary structures, texture, diagenesis and facies. The studied interval is from 1760 to 1913 m and includes Kangan major sequences bounded by the Dashtak Formation at the top and by the Dalan Formation at the base. The extracted data have been interpreted to identify the main FMI signatures that allow a perfect recognition of several sedimentologic, diagenetic or reservoir-oriented feature associations. The images have been successfully matched to the core descriptions to provide a correlative side by side setting between geologic and FMI facies. Most of the main structures, textures or lithologies observed on cores and thin section have been identified on images. This study has yielded to identification and characterisation on image logs of the 12 FMI facies (FF) defined for the entire Kangan formation (Table 1).

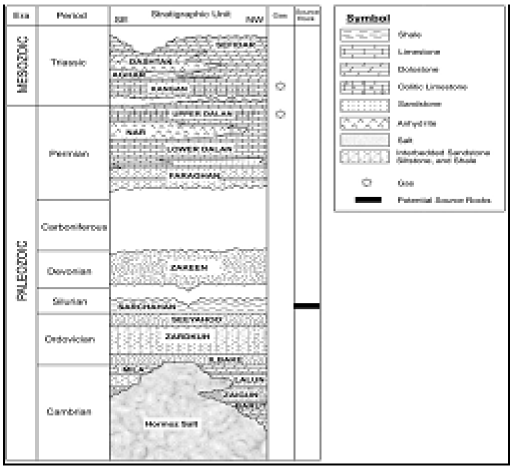

Fig 2: Stratigraphic chart (Formations and main lithology) of the South Pars gas field in the Persian Gulf

Lithology and fabric

The FMI tool is particularly sensitive to the textural changes that characterize the different rock fabrics and micro-resistivity variations are influenced by mineralogy, porosity, grain size, cementation and type of pore fluid. Resistivity of non porous sedimentary rocks is specific to their mineralogy. As examples anhydrite has a resistivity which is comprised between 10^4 and 10^{14} ohm-m and it appears as the more resistive lithology with a white colour in FMI logs. shales have a resistivity which is comprised between 0.5 and 60 ohm-m and are the more conductive lithology and their FMI signatures appear dark tint. The contrast of resistivity between dense limestone and dense dolomite is less distinguishable, around 1000 ohm-m for the two once. Carbonates appear as a wide colour range between light yellow and dark red. A distinction can be considered that corresponds to the more frequent association between dolomite and anhydrite rather than between limestone and anhydrite. It is easy to distinguish anhydrite from dolomite on static FMI images, but difficult without particular processing or electric log comparison to discriminate dolomite from limestone. Within limestones, grain-supported beds are less resistive and generally display foreset bedding, except when they are totally plugged by strong cement. Mud-supported intervals are more resistive, with white spots corresponding probably to allochems, and dark spots probably related with vugs. Matrix porosity allows fair conductive FMI response.

Within dolostones, grain-supported beds are more or less resistive, depending on anhydrite cementation and display occasional foreset bedding, but mud-supported intervals are generally less resistive. Resistivity is in adequation with crystal shape and size that influence intercrystalline and matrix porosity development.

Sedimentary structures

The FMI tool due to its high resolution shows a good visualisation of several types of sedimentary structures: bed boundaries, thickness, internal structures and bioturbation. Bed boundaries are marked by abrupt or gradational and relatively high resistivity contrasted lines yielding bedding organisation. These boundaries define bodies, on which aspect and thickness could be established and measured. The internal structures are easily identifiable in dynamic normalisation by the resistive contrast existing between cross-beds (or lamination sets) and their clayey bounding layers. Some images show recognisable shape of bioturbation, particularly for sub-vertical burrows, which are more or less parallel to the borehole axis.

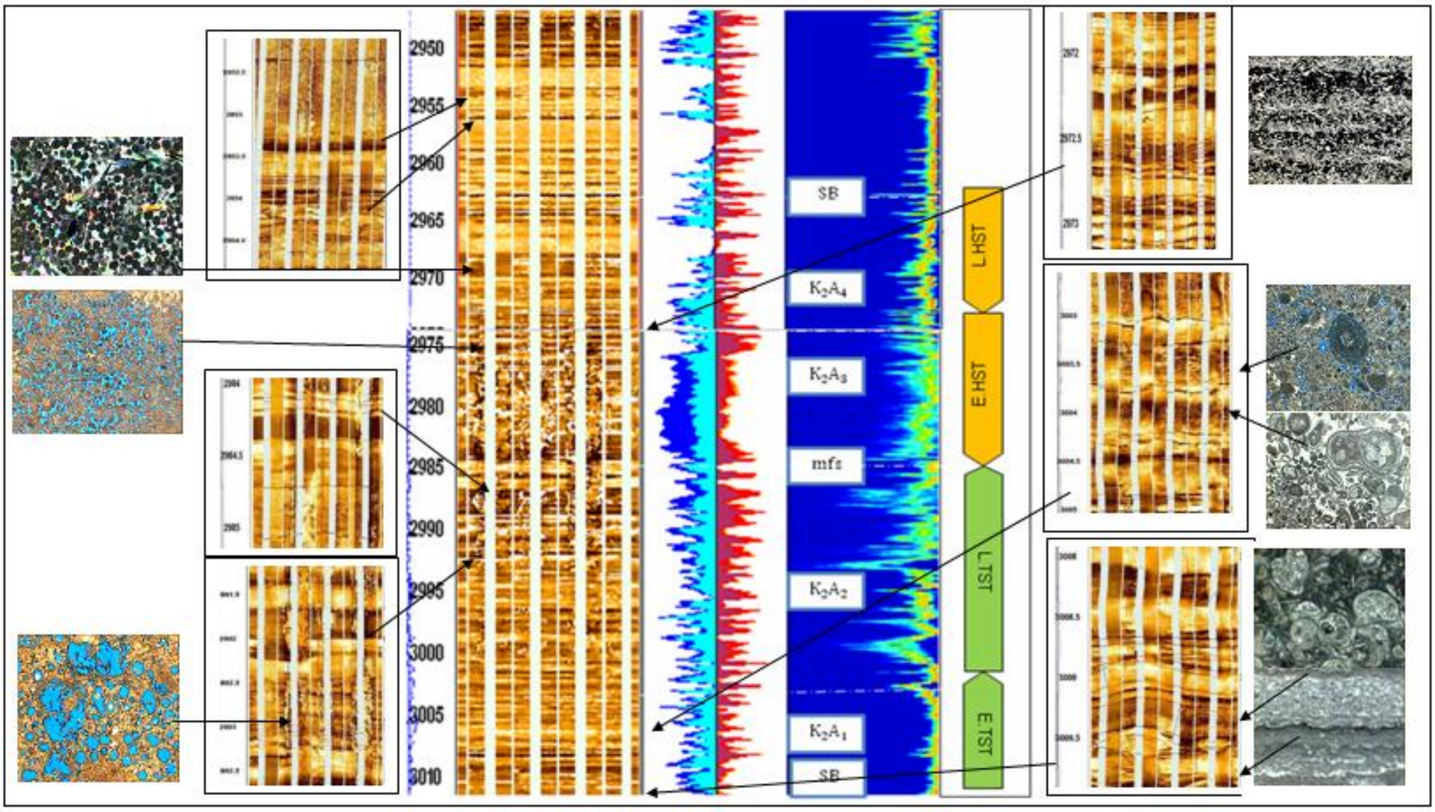

Fig 3: Sequence stratigraphy and reservoir characteristics in K_2 interval, W1, kangan formation

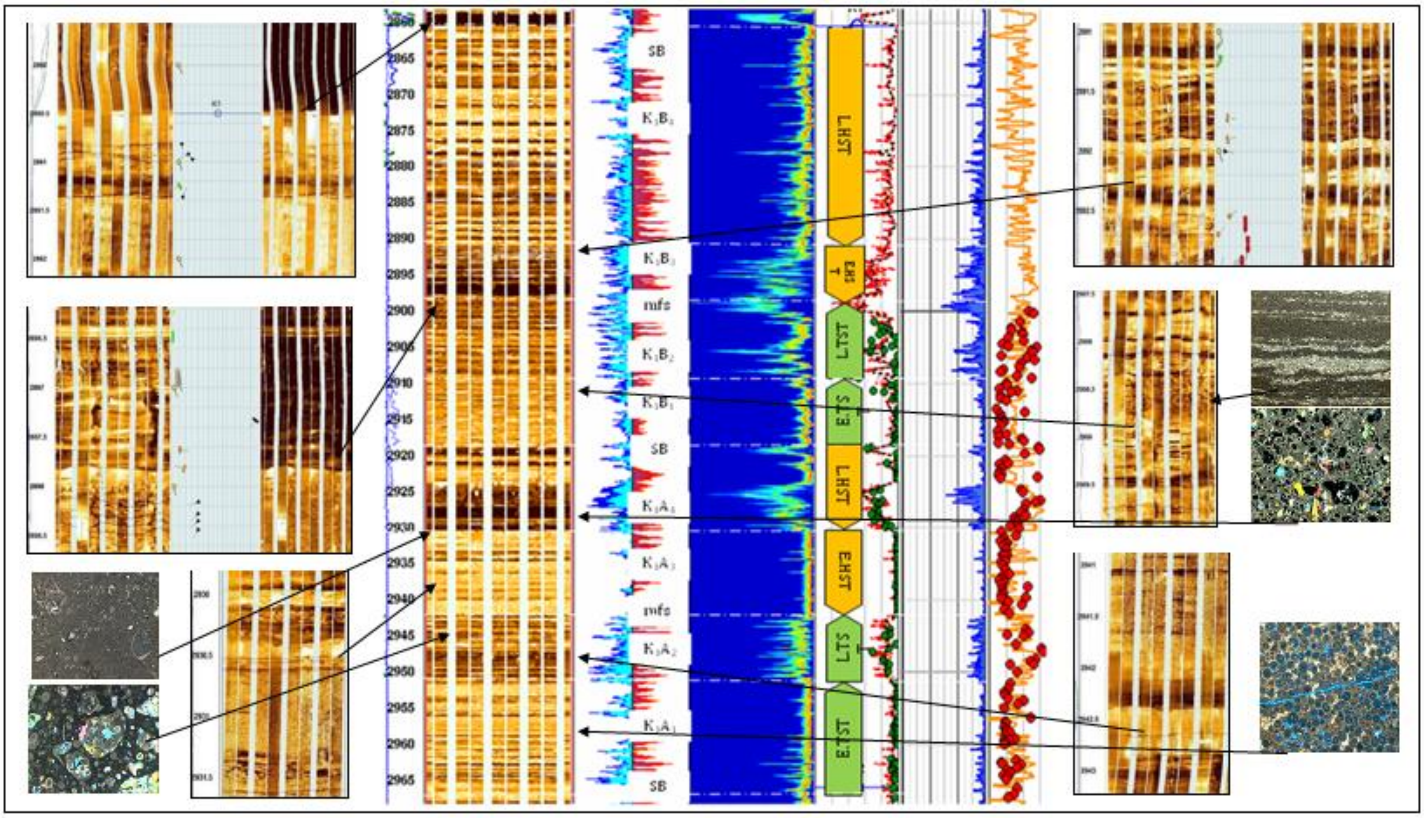

Fig 4: Sequence stratigraphy and reservoir characteristics in K_1 intervalW1, kangan formation

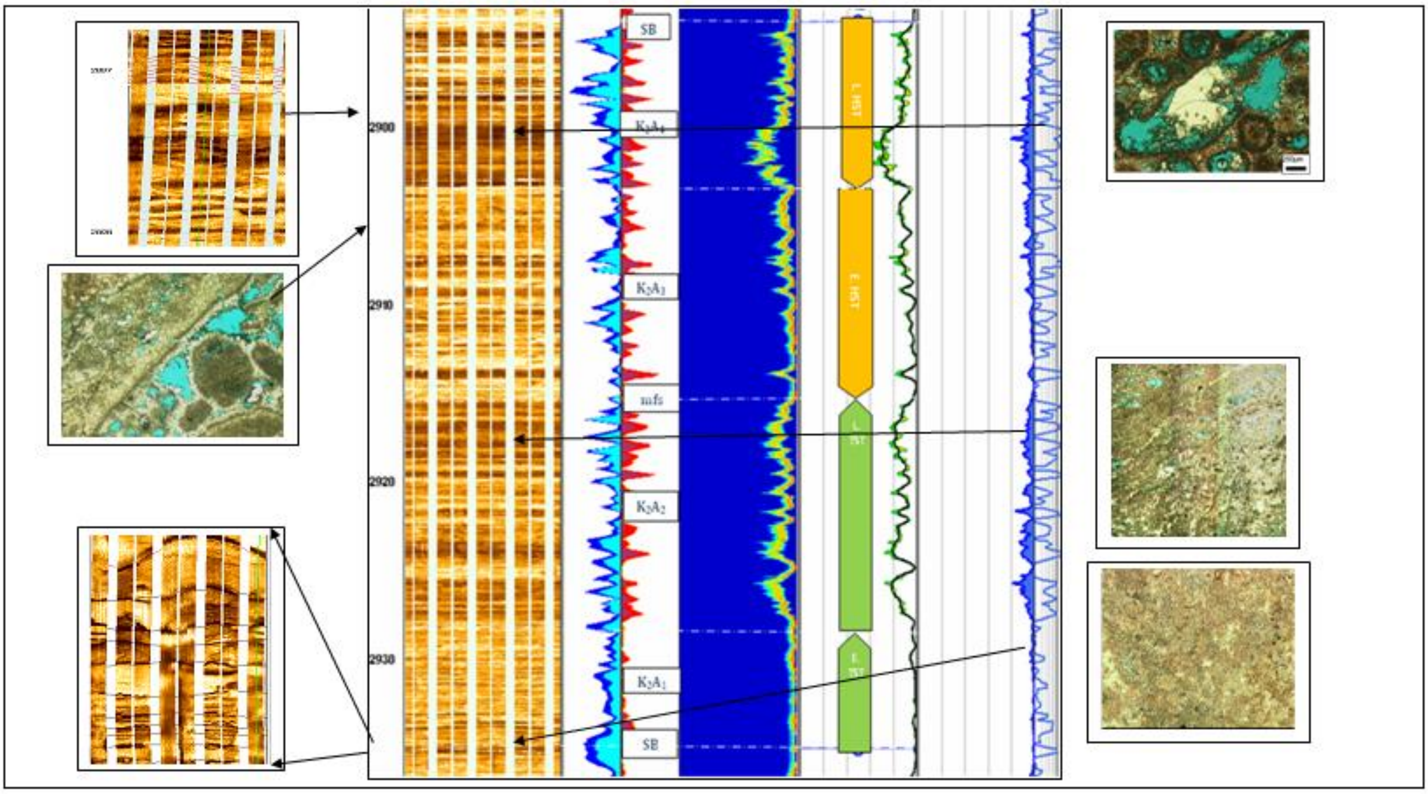

Fig 5: Sequence stratigraphy and reservoir characteristics in K_2 interval, W2, kangan formation

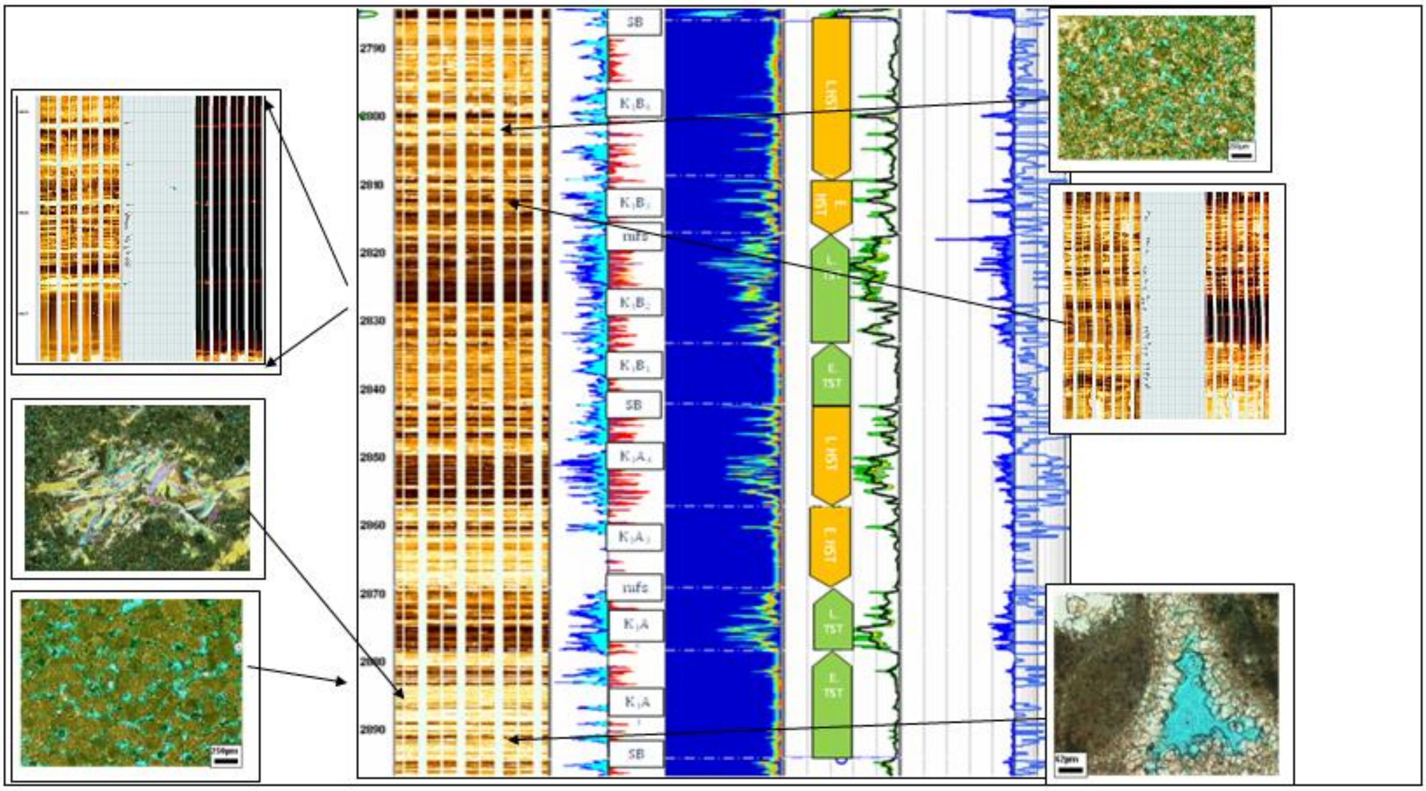

Fig 6: Sequence stratigraphy and reservoir characteristics in K1 interval, W2, kangan formation

Table 1: main facies and other characteristic of Kangan Formation

No.	Facies	Maine cement type	Maine porosity type	Maine diagenetic process	Dep.environment
1	Anhydritic dolomudstone, dolowackestone (FF1	Dolomite, anhydrite	Interparticle,fenestral Intercrystaline	Dolomitization, anhydrite patches,neomorphism	Res.lagoon, Tidalflat
2	Stromatolite/thrombolit Boundstone with anhydrite cement(FF2)	Anhydrite, calcite	interparticle,Intercrystaline, fenestral	Compaction, anhydrite patches,	Upper Intertidal
3	Dolomitic skeletal, Wackstone Packstone with Interaclast and burrow (FF3)	Anhydrite, Calcite,dolomite	Intercrystaline,Inter/aparticle, Vuggy,moldic	Dolomitization, anhydrite patches, Compaction	Lagoon,Intertidal
4	Medium to coarse grained cross-bedded ooid grainstone/ooid dolograinstone with bioclast(FF4).	Calcite, Dolomite	Inter/aparticle, Vuggy,moldic	Dissulution, Dolomitization Compaction	Lower Intertidal Ooid shoal
5	Coarse grained skeletal, interaclast grainstone and packstone with lithoclasts (FF5)	Calcite, Dolomite	Inter/aparticle, Vuggy, moldic,shelter	Dissulution, Dolomitization Compaction,replacement, thin fractures,	Lower intertidal, Seaward shoal
6	Fine grained ooid packstone to grainstone with peloids and lithoclasts (FF6)	Calcite, Dolomite	interparticle, moldic intercrystaline,vuggy	Dissulution, replacement stylolite, Dolomitization	Lagoon
7	Fine grained anhydritic, ooid packstone to grainstone with peloids, (FF7).	Anhydrite, Calcite,dolomite	Inter/aparticle, Vuggy,moldic	anhydrite patches, Dolomitization, Compaction,	Lower intertidal
8	Massive, nodular or laminated anhydrite bedding (FF8).	Dolomite, anhydrite	interparticle, intercrystaline	plugged by anhydrite, Dolomitization,	Supratidal
9	Medium to coarse grianed crossbedded ooid, skeletal grainstone with anhydrite cement (FF9).	Calcite, Dolomite	Inter/aparticle, Vuggy,moldic	Dissulution, replacement stylolite, Dolomitization	Lower intertidal, Ooid shoal
10	Limy mudstone to wackestone,with anhydrite cement (FF10)	Calcite, Dolomite	interparticle, intercrystaline	Dolomitization, neomorphism	Res.lagoon, Tidalflat
11	Intraclast breccia with anhydrite cement(FF11)	Blocky anhydrite	Fracture,Interparticle, intercrystaline	plugged by anhydrite, Compaction,	Supratidal
12	Shaly dolomudstone with black lamination(FF12)	Calcite, Dolomite	interparticle, intercrystaline	Compaction, Dolomitization,	Tidalflat

Table 2: Parameters of various depositional units of K_2 depositional sequence

sequence	Sys. tracts	Main Facies	Res. chac.	Major Surface	Depth(m)
K_2A	HST			SB	1863
		Dolomitized grainstones with	low	K_2A_4	1874 to 1852
		Dolomitic limestones	high	K_2A_3	1885 to 1874
				mfs	1885
	TST	Conductive grainstone	high	K_2A_2	1903 to 1885
		Dolomitic mud-Supported with Anhydrite	low	K_2A_1	1913 to 1903
				SB	1913

Table 3: parameters of various depositional units of K_1 depositional sequence

sequence	Sys.tracts	Main Facies	Res. chac.	Major Surface	Depth(m)
K_1B	HST			SB	1760
		Dolopackstones/grainstones, anhydrite	Low	K_1B_4	1790 to 1760
		Peloidal, lithoclastic dolograinstone	Fair, low	K_1B_3	1798 to 1790
				mfs	1798
	TST	Ooid, bioclast grainstone	High	K_1B_2	1809 to 1798
		Mud-supported limestone	Low	K_1B_1	1819 to 1809
				SB	1819
K_1A	HST	Bioturbated oolithoclastic mud/grainstones	High, fair	K_1A_4	1829 to 1819
		Peloidal lithoclastic grain/mudstone,	Low, fair	K_1A_3	1842 to 1829
				mfs	1842
	TST	Dolomitized grainstone	Fair, good	K_1A_2	1851 to 1842
		Mud-supported with anhydrite	Low	K_1A_1	1867 to 1851
				SB	1867

By anhydrite infilling, horizontal burrows appear generally as rounded white shades. The other bioturbations, more easily identifiable when they are abundant, generate a fuzzy textural response, always composed by dark patches and white spots generally poorly defined. Frequent destabilisation or collapse breccia is recognisable with the strong contrast which occurs between the resistivities of the matrix and of the elements.

Diagenetic process

Stylolites and dissolution seams often contain residual minerals such as clay or other minerals. They might be invaded by drilling mud. They generally occur in compact cemented carbonate formations. Because of their conductive mineralogical contents, they appear as black irregular lines on resistivity images. Physical compaction determined by conductive or resistive point/patch that is arranged in a specific direction. Strong cementation appears on the FMI picture as a homogeneous response. In the Kangan Formation the main cementation phases are: calcitisation, dolomitisation that difficult to characterise because of the weak contrast with the surrounding carbonates and anhydritisation that very easily identifiable according to its strong natural resistivity. The main dissolution phases that lead to porosity development reveal conductive-dominated FMI response. Moldic or vuggy porosity develop mottled structure on image log. More homogeneous conductive layer results from well connected porosity such as intergranular or intercrystalline porosity. Open fractures and vertical fractures induced by drilling that filled by shale and mud appear as black conductive features. Cemented fractures, generates white resistive features.

The sedimentological study of FMI logs, cores and thin sections led to the identification of 12 FMI facies for the entire Kangan Formation within studied wells (1 and 2) (Table1). Some of the lithofacies have a specific signature on image logs but many show diagenesis overprinting or stumping the original response. Considering these recongnized facies occurre environments including sabkha evaporitic, arid peritidal settings, restricted lagoon, carbonate sand shoal (leeward shoal, ooid shoal and seaward shoal) and open sea, indicating deposition in an extensive homoclinal ramp.

Sequence stratigraphy and reservoir characteristics

In the earlier studies using the parameters such as lithology, facies and reservoir characteristics, the Kangan formation is subdivided into two distinct reservoir units including the K_1 and K_2. The K_2 unit (Lower interval) main lithology consists of dolomite (in the upper part) and limestone (in the lower part). The K_1 unit (Upper interval) represents an alternation between dolostone, limestone and anhydrite layers.

Based on this study the Kangan Formation has been subdivided into 3 major sequences (K_1A, K_1B and K_2A) with various internal depositional sequences. K_2A depositional sequence corresponds to the Lower Kangan Formation with a HST and TST as a complete transgressive and regressive third-order cycle system tracts bounded by two sequence boundary surface (type 1), mfs and 4 small depositional units (Table 2) (Fig. 3).

The K_1 interval consists of K_1A and K_1B sequence, three significant sequence boundaries, two mfs and eight distinct depositional units. The sequence is attributed as a complete transgressive–regressive cycle consisting of the transgressive (TST) and highstand (HST) systems tracts (table 3, fig 4).

Conclusions

The sedimentological study of all data led to the identification of 12 FMI facies for the entire Kangan Formation. Lithofacies characterisation on FMI loggings can be used for comprehension and extrapolation of the non cored wells but a sedimentological callibration is needed to avoid misinterpretation.

Reservoir quality varies between depositional sequences, depending upon their original facies, depositional setting and their further specific diagenetic alterations.

Based on the description all data, three major composite depositional sequences have been defined: K_1A, K_1B and K_2A. They have been further subdivided into 12 distinctive depositional units 6 tight (low reservoir characteristics) and 6 conductive (high reservoir characteristics).

The K_2 depositional sequence contains an almost equal distribution of limestone and dolostone lithologies. The K_2 reservoir is the composite depositional sequence, with moldic and intergranular porosity. The K_1 sequences are relatively poor reservoir and consist of mud supported sediments. The K_2A_3 unit is the best poros interval.

Reservoir portion is characterised by the calcareous and dolomitic intervals, separated by several tight dolomitic levels. Late TST and early HST stages correspond to depositional units K_2A_2, K_2A_3, K_1A_2, K_1B_2 and K_1B_3, are calcareous in nature. Late TST is characterised firstly by a good development of moldic and intergranular porosity linked with bioclast dissolution, secondly by tight thrombolytic limestones. Early HST contains lithoclastic material that has been subjected to strong moldic dissolution. Moldic spaces are locally reduced by the precipitation of scattered dolomite cements. Intergranular porosity is also present, and is volumetrically less important than moldic porosity.

Late HST stages are marked by K_2A_4, K_1A_4 and K_1B_4 and tight in nature, all original spaces have been completely occluded by anhydrite. The reservoir characteristics generated in K_2A_3 are due to important dissolution and recrystallisation, resulting in a complex porous network. The K_1 interval seals are found in the K_1A_1, K_1B_1, K_2A_4 and K_2A_1 depositional sequences (early TST and late HST stages) represent shallow marine environments and associated with evaporite sediment.

All reservoir intervals represent the settling of oolitic and locally bioclastic. Oomoldic dissolution is common within limestone portions, whereas intergranular porosities are more common within dolomitic sections.

Acknowledgements

This work was supported by the POGC (Pars Oil and Gas Company of Iran). The authors thank POGC for some data preparation, and permission to publish this paper.

References

1) Aali & Rahmani, 2011, Evidences for secondary cracking of oil in South Pars field, Persian Gulf, Iran, Journal of Petroleum Science and Engineering, 76 (2011) 85–92

2) Aali J, Rahimpour-Bonab H, Kamali MR. 2006, Geochemistry and origin of the world's largest gas field from Persian Gulf, Iran, journal of petroleum science and engineering, Vol.50, pp.161–175.

3) Al-Jallal, I. A., 1987, Diagenetic effects on reservoir properties of the Permian Khuff Formation in eastern Saudi Arabia: Society of Petroleum Engineers 6th Middle East Oil Show, p. 465–476.

4) Alsharhan, A. S., and Nairn, A. E. M., 1997, Sedimentary Basins and Petroleum Geology of the Middle East, (Netherlands: Elsevier)

5) Arab Oil and Gas Magazine, 2003, The Arab Petroleum Research Center, AOGM, vol.4, pp. 14–16.

6) Bhavana, P.R and Rao, M.V, 2001, Application of Fullbore Formation MicroImager in recognising structural elements, sedimentary features and depositional environments, case studies from Krishna-Godavari basin, India, ONGC, unpublished report, pp. 1- 41.

7) Chai Hua, Li Ning, Xiao Chengwen, Liu Xingli, Li Duoli, Wang Caizhi, and Wu Dacheng 2009, Automatic discrimination of sedimentary facies and lithologies in reef-bank reservoirs using borehole image logs Applied Geophysics, Vol.6, pp. 17-29.

8) Dunham¬¬¬, R.J., 1962, Classification of carbonate rocks according to depositional texture, American Association of Petroleum Geologists Memoir1, pp. 108–121.

9) Edgell, H.S. 1996, Salt tectonics in the Persian Gulf basin, In: Alsop, G.L., Blundell, D.L. & Davison, I.(eds) Salt Tectonics. Geological Society, London, Special Publications, 100, 129–151.

10) Esrafili-Dizaji, B. and Rahimpour-Bonab, H., 2009, Effects of depositional and diagenetic characteristics on carbonate reservoir quality: a case study from the South Pars gas field in the Persian Gulf Pet. Geosci. 15 325–44

11) Kashfi, M.S., 1992, Geology of the Permian supergiant gas reservoirs in the greater Persian Gulf area, Petroleum Geology Vol.15, 465–480.

12) Kashfi, MS., 2000, Greater Persian Gulf Permian-Triassic stratigraphic nomenclature requires study, Journal of Oil and Gas, Tulsa 6, 36–44.

13) Konyuhov, A. I. and Maleki, B., 2006, The Persian Gulf basin: geological history, sedimentary formations, and petroleum potential Lithol. Miner. Resources 41 344–61

14) Lovell, M. A., Harvey, P. K., Brewer, T. S., Williams, C., Jackson, P. D., and Williamson, G., 1997, Application of FMS images in the Ocean Drilling Program an overview (in geological evolution of ocean basins, results from the Ocean Drilling Program), geological Society Publications, pp 287–303.

15) Moradpour M, Zamani Z and Moallemi, S. A., 2008, Controls on reservoir quality in the lower Triassic Kangan formation, southern Persian Gulf, J. Pet. Geol. 31, 367–86

16) Newberry, B. M., Grace, L. M., and Stief, D. D., 1996, Analysis of carbonate dual porosity systems from borehole electrical images in Proceedings Permian Basin Oil and Gas Recovery Conference, Society of Petroleum Engineers, pp.123–120.

17) Nurmi, R., Charara, M., Waterhouse, M., and Park, R.,1990, Heterogeneities in carbonate reservoirs: detection and analysis using borehole electrical imagery: in Geological Applications of Wireline Logs, Geological Society, London, Special Publications, Vol. 48, pp.95–111.

18) Prensky, S. E., 1999, Advances in borehole imaging technology and applications: in Borehole Imaging: Applications and Case Histories, Geological Society Special Publications, Vol.159, pp.1– 43.

19) Prilliman, J., Bean, C., Hashem, M., Bratton, T., Fredette, M. A., and Lovell, J. R., 1997, A comparison of wireline and LWD resistivity images in the Gulf of Mexico: Transactions of the SPWLA Annual Logging Symposium, 38, 111.

20) Rahimpour-Bonab, H., 2007, A., procedure for appraisal of a hydrocarbon reservoir continuity and quantification of its heterogeneity, J. Pet. Sci. Eng. 58 1–12

21) Rahimpour-Bonab, H., Asadi-Eskandar, A., Sonei, A., 2009, Controls of Permian-Triassic Boundary over Reservoir Characteristics of South Pars Gas Field, Persian Gulf, Geol. J. 44, 341–364.

22) Rahimpour-Bonab, H., Esrafili-Dizaji, B., Tavakoli, V., 2010, Dolomitization and anhydrite precipitation in permotriassic carbonate at the South Pars Gas field, controls on reservoir quality, Journal of Petroleum Geology, Vol.33, pp. 43-66.

23) Russell, S. D., Akbar, M., Vissapragada, B., and Walkden, G. M., 2002, Rock types and permeability prediction from dipmeter and image logs; Shuaiba reservoir (Aptian), Abu Dhabi, AAPG Bulletin, Vol. 86/10, pp. 1709-1732.

24) Schlumberger, 2004, FMI Fullbore Formation MicroImager, www.slb.com,

25) Serra, O., 1989, Formation microscanner image interpretation Schlumberger Educational Service, Houston, 1 – 5.

26) Sharland, P.R., Archer, R., Casey, D.M., Davies, R.B., Hall, S.H., Heward, A.P., Horbury, A.D., Simmons, M.D., 2001, Arabian plate sequence stratigraphy. Geo Arabia Special Publication, Gulf Petro Link, Bahrain, Vol. 2, 371 pp.

27) Standen, E., Nurmi, R., El-Wazeer, F., and Ozkanli, M., 1993 Quantitative applications of wellbore images to reservoir analysis: Transactions of the SPWLA Annual Logging Symposium, 34.

28) Szabo, F., Kheradpir, A., 1978, Permian and Triassic stratigraphy, Zagros basin, South-West Iran, Petroleum Geology Vol.1, pp.57–82.

29) Tavakoli, V., Rahimpour-Bonab H and Esrafili-Dizaji, B., 2011, Diagenetic controlled reservoir quality of South Pars gas field, an integrated approach Geoscience 343 55–71

30) Ziegler, 2001, Late Permian to Holocene Paleofacies Evolution of the Arabian Plate and its Hydrocarbon Occurrences, Geo Arabia, Vol. 6, 3, Gulf Petro Link, Bahrain 445.